crystals

MDPI

Article

Mechanical Properties, Electronic Structures, and Debye Temperature of Ni_xB_y Compounds Obtained by the First Principles Calculations

Kaiming Wang [1], Dong Du [1], Baohua Chang [1,*], Yuxiang Hong [1], Jiang Ju [2], Shuting Sun [3] and Hanguang Fu [3]

1 State Key Laboratory of Tribology, Department of Mechanical Engineering, Tsinghua University, 1 Qing Hua Yuan, Haidian District, Beijing 100084, China; kmwangbjut@163.com (K.W.); dudong@tsinghua.edu.cn (D.D.); hongyuxiang@tsinghua.edu.cn (Y.H.)

2 School of Materials Science and Engineering, Shanghai Jiao Tong University, Shanghai 200240, China; jujiang1990@sjtu.edu.cn

3 School of Materials Science and Engineering, Beijing University of Technology, Beijing 100124, China; sst@emails.bjut.edu.cn (S.S.); hgfu@bjut.edu.cn (H.F.)

* Correspondence: bhchang@tsinghua.edu.cn; Tel.: +86-10-6278-1182; Fax: +86-10-6277-3862

Received: 23 October 2018; Accepted: 27 November 2018; Published: 30 November 2018

Abstract: Mechanical properties, electronic properties, and Debye temperatures of Ni_xB_y (Ni_3B, Ni_2B, Ni_4B_3 and NiB) compounds were obtained by the first principles calculations based on the density functional theory (DFT). The results showed that the formation enthalpy of the Ni_xB_y compounds were stable with negative formation enthalpy. NiB had the largest B, G, and E, and the smallest υ; it also had the highest hardness (10.8 GPa) and Debye temperature (681.8 K). Ni_4B_3 had the strongest anisotropy. It was found that the valence bonds of the Ni_xB_y compounds studied were composed of both metal bond and covalent bond, and the mechanical properties and Debye temperature of the Ni_xB_y compounds increased with the increase of the B atomic ratio.

Keywords: Ni_xB_y compounds; first-principles; mechanical properties; electronic structures; Debye temperature

1. Introduction

Nickel-based alloy powders are widely adopted in surface modification due to their good wettability, superior high-temperature properties, and moderate price [1,2]. Nickel (Ni) and boron (B) can generate different Ni-B binary compounds, which have an important effect on the properties of the coatings [3]. Appropriate B can prevent liquid metal oxidation and reduce the inclusion in the coating [4]. However, excessive B will increase the crack susceptibility of the coatings and should be avoided [5]. Researchers have carried out a lot of experimental studies on the properties of Ni-B binary compounds [6–9]. Laser cladding is a new type of surface modification technology, in which some powders of special properties are cladded onto the surface of a substrate [10,11]. Compared with other traditional surface modification technologies, it can create coatings with better mechanical properties [12,13]. However, the studies are very limited on the effect of Ni-B binary compounds on the Ni-based laser cladding layer properties. It is very expensive to analyze the effects of different Ni-B contents by experimental method.

In recent years, computational materials science has been developing rapidly with the continuous development of computer technology. It can be used to predict the structure and properties of materials, improve efficiency, and reduce cost in production [14]. The first principles method based on density functional theory has been used to investigate the properties of Ni_xB_y compounds. Researchers

have studied some Ni_xB_y compounds in different systems. Shein et al. [15] calculated the lattice constant, magnetic properties, and formation energy of Ni_3B, which indicated that the strong stability of Ni_3B was due to the strong Ni–B hybridization. Zhou et al. [16] researched the stability, electronic, and structural properties of X_2B (X = Cr, Mn, Fe, Co, Ni, Mo, and W) compounds. Zhou et al. [17] investigated the electronic structure and mechanical properties of NiB, which is predicted to be a promising interphase material for future ultrahigh-temperature ceramic fiber reinforced ceramic matrix (UHTCF/UHTC) composites. However, there is no literature that studied the effects of different ratios of Ni to B on the mechanical properties, electronic properties, and Debye temperature of Ni_xB_y compounds.

In our previous research work, Ni-based composite coating was obtained by Ni-based self-fluxing alloy powders [18], but there was no deep and comprehensive research on the properties of Ni_xB_y compounds. In this study, the mechanical properties, electronic properties, and Debye temperature of Ni_xB_y compounds were calculated by using the first-principles. The obtained results could provide guidance for the properties of Ni-based laser cladding layers.

2. Methods

In this paper, mechanical properties, electronic properties, and Debye temperature of Ni_xB_y compounds were calculated based on density functional theory (DFT) by CASTEP [19]. Kohn-Shan equation was calculated by Perthew-Burke-Ernzerhof (PBE) method in the generalized gradient approximation (GGA). The ultrasoft pseudopotential was used to describe the interactions between valence electrons and ionic cores [20]. The valence electrons of Ni and B are $3p^6 3d^8 4s^2$ and $2s^2 2p^1$, respectively. The crystals structures of these Ni_xB_y compounds are shown in Figure 1. The coordinates of Ni_3B are Ni (0.180, 0.063, 0.156), (0.028, 0.250, 0.633) and B (0.618, 0.750, 0.561). The coordinates of Ni_2B are Ni (0.170, 0.330, 0) and B (0.500, 0.500, 0.250). The coordinates of Ni_4B_3 are Ni (0.175, 0.064, 0.346), (0.019, 0.250, 0.869) and B (0.887, 0.250, 0.420). The coordinates of NiB are Ni (0, 0.147, 0.250) and B (0.5, 0.067, 0.750). To optimize equilibrium crystal parameters and the atomic position of these Ni_xB_y compounds, the Broyden–Fletcher–Goldfarb–Shannon (BFGS) algorithm was used. According to the convergence results, the maximum cut-off energy of the plane wave was taken as 500 eV. The Monkhorst–Pack was used to characterize energy integration in the first irreducible Brillouin zone (BZ), and the *k* point mesh was adopted 16 × 16 × 16. The total energy changes during the optimization process were finally converged to 2×10^{-6} eV, and the maximum force on the atoms was below 0.001 eV/Å.

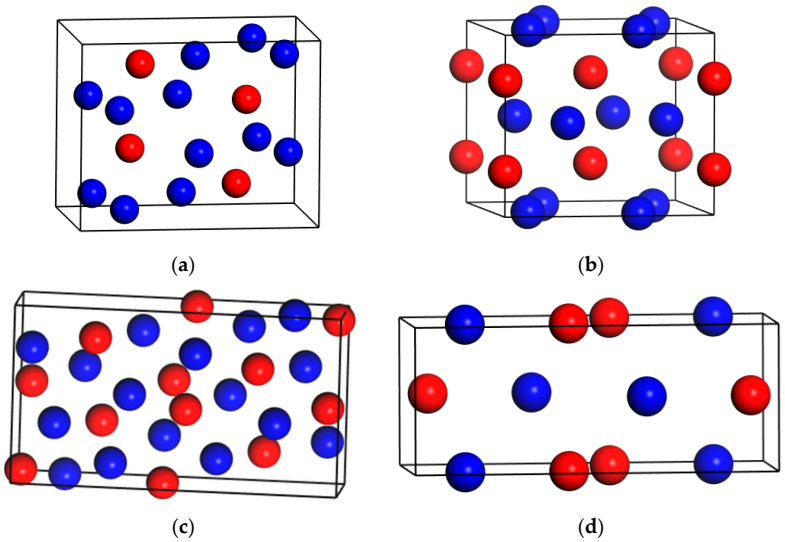

Figure 1. The crystal structure of Ni_xB_y compounds (red balls represent B atoms, blue balls represent Ni atoms) (**a**) Ni_3B; (**b**) Ni_2B; (**c**) Ni_4B_3; (**d**) NiB.

The thermodynamic stability of the compounds is related to formation enthalpy. A compound is thermodynamically stable when the formation enthalpy of the compound is negative. The smaller the values of the formation enthalpy, the more stable is the compound. The formation enthalpy can be calculated by following equation [21]:

$$\Delta_r H_m(Ni_xB_y) = \frac{E_{total}(Ni_xB_y) - x \cdot E_{bulk}(Ni) - y \cdot E_{bulk}(B)}{n} \quad (1)$$

where $\Delta_r H_m(Ni_xB_y)$, E_{total}, E_{bulk}, and n are the formation enthalpy, the total energy, the chemical potential, and the sum of the number of atoms, respectively.

3. Results and Discussion

3.1. Stability

To ensure reliability of the calculation, the structure of crystal was first optimized and then the lattice parameters under 0 K were obtained. Optimized lattice parameters are listed in Table 1. The error between our results and predecessors calculation data was less than 3.0%, which proved that the parameters used in this research were reliable. The formation enthalpy of Ni_xB_y compounds calculated using Equation (1) is shown in Table 1. The formation enthalpies of Ni_3B, Ni_2B, Ni_4B_3, and NiB are −32.819 kJ/mol, −35.848 kJ/mol, −36.026 kJ/mol, and −32.547 kJ/mol, respectively. The formation enthalpies are all negative, which indicate that these Ni_xB_y compounds are thermodynamically stable. Ni_4B_3 has more thermodynamic stability than other compounds because its formation enthalpy is the lowest.

Table 1. The optimized parameters of Ni_xB_y compounds.

Compound	Space Group	Crystal Type	Lattice Constants (Å)			Cell Angles (°)			Formation Energy (kJ/mol)
			a	b	*c*	α	β	γ	
Ni	Fm-3m	cubic	3.530 3.520 [a]	3.530 3.520 [a]	3.530 3.520 [a]	90.0	90.0	90.0	
Ni_3B	Pnma	orthorhombic	4.417 4.429 [b]	6.671 6.659 [b]	5.199 5.108 [b]	90.0	90.0	90.0	−32.819
Ni_2B	I4/mcm	tetragonal	4.991 4.991 [c]	4.286 4.284 [c]	4.991 4.991 [c]	90.0	90.0	90.0	−35.848
Ni_4B_3	Pnma	orthorhombic	3.005 2.981 [d]	6.603 6.568 [d]	12.011 11.954 [d]	90.0	90.0	90.0	−36.026
NiB	Cmcm	orthorhombic	2.991 2.927 [e]	2.982 2.963 [e]	7.338 7.394 [e]	90.0	90.0	90.0	−32.547
B	R-3m	rhombohedral	4.899 4.924 [f]	4.899 4.924 [f]	12.551 12.609 [f]	90.0	90.0	120.0	

[a] Ref. Cal. [22]; [b] Ref. Cal. [23]; [c] Ref. Cal. [16]; [d] Ref. Cal. [24]; [e] Ref. Cal. [17]; [f] Ref. Cal. [25].

3.2. Mechanical Properties

3.2.1. Elastic Constant and Elastic Modulus

Mechanical properties are related to elastic constants C_{ij}, which are determined by the bond strength between the atoms, and are the scientific basis in designing and developing new materials [26]. The stress-strain method is used to evaluate the elastic constants of these Ni-B compounds. The strain-stress curve is described by the Hooke's law, which is given by following equation [27]:

$$\sigma_{ij} = C_{ijkl}\varepsilon_{kl} \quad (2)$$

where σ_{ij} is the stress tensor, ε_{kl} is the strain tensor, and C_{ijkl} is the elastic constant tensor which is a 6×6 matrix (36 elements in general cases). The elastic constants are calculated as follows [26]:

$$\begin{pmatrix} \sigma_1 \\ \sigma_2 \\ \sigma_3 \\ \tau_1 \\ \tau_2 \\ \tau_3 \end{pmatrix} = \begin{pmatrix} C_{11} & C_{12} & C_{13} & C_{14} & C_{15} & C_{16} \\ & C_{22} & C_{23} & C_{24} & C_{25} & C_{26} \\ & & C_{33} & C_{34} & C_{35} & C_{36} \\ & & & C_{44} & C_{45} & C_{46} \\ & & & & C_{55} & C_{56} \\ & & & & & C_{66} \end{pmatrix} \begin{pmatrix} \varepsilon_1 \\ \varepsilon_2 \\ \varepsilon_3 \\ \gamma_1 \\ \gamma_2 \\ \gamma_3 \end{pmatrix} \quad (3)$$

where σ_i and τ_i are the normal stress and the shear stress, respectively. C_{ij} is the elastic constant. ε_i and γ_i are the shearing strain and the normal strain, respectively.

Born–Huang lattice dynamical theory can judge the mechanical stability of the compounds and it needs to meet the following criteria [28–30]:

Orthorhombic phases (for Ni_3B, Ni_4B_3, and NiB)

$$\begin{aligned} &C_{11} > 0, C_{11}C_{22} > C_{12}^2, C_{11}C_{22}C_{33} + 2C_{12}C_{13}C_{23} - C_{11}C_{23}^2 - C_{22}C_{13}^2 - C_{33}C_{12}^2 > 0, \\ &C_{44} > 0, C_{55} > 0, C_{66} > 0 \end{aligned} \quad (4)$$

Tetragonal phase (for Ni_2B)

$$\begin{aligned} &C_{11} > 0, C_{22} > 0, C_{33} > 0, C_{44} > 0, C_{55} > 0, C_{66} > 0, \\ &C_{11} + C_{33} - 2C_{13} > 0, \\ &2(C_{11} + C_{12}) + C_{33} + 4C_{13} > 0 \end{aligned} \quad (5)$$

Table 2 shows the elastic constants of Ni_xB_y compounds. Examining the data against Equations (2)–(3), it can be found that these Ni_xB_y compounds meet the criteria of mechanical stability. Therefore, Ni_3B, Ni_2B, Ni_4B_3, and NiB are mechanically stable structures.

Table 2. The calculated elastic constants (in GPa) of Ni_xB_y compounds.

Compounds	Elastic Constants								
	C_{11}	C_{12}	C_{13}	C_{22}	C_{23}	C_{33}	C_{44}	C_{55}	C_{66}
Ni_3B	348.6	184.1	161.7	340.8	184.4	363.4	132.6	96.7	112.4
Ni_2B	405.7	207.6	165.5	408.6	167.1	416.0	102.9	102.8	138.9
Ni_4B_3	379.3	201.1	210.2	417.4	169.2	401.5	110.8	147.8	140.5
NiB	352.3	170.0	194.7	508.5	178.1	419.9	137.2	111.2	129.4

Elastic properties are mainly determined by elastic modulus. Bulk modulus (B), Young's modulus (E), shear modulus (G), and Poisson's ratio (v) can be calculated by Voigt-Reuss-Hill (VRH) approximation [31]. VRH approximation is mainly based on the symmetry of the crystal, which is the average value of the lower limit value of Voigt and the upper limit value of Reuss. VRH approximation provides methods to estimate the mechanical properties of compounds from elastic constants [32]. The equations are as follows [33,34]:

$$B = \frac{1}{2}(B_V + B_R) \quad (6)$$

$$G = \frac{1}{2}(G_V + G_R) \quad (7)$$

$$E = \frac{9B \cdot G}{3B + G} \quad (8)$$

$$v = \frac{3B - 2G}{2(3B + G)} \quad (9)$$

where B_V, B_R, G_V, and G_R are the bulk modulus and the shear modulus calculated by Voigt and Reuss, respectively.

The calculation results are shown in Table 3. Bulk modulus is a parameter that reflects the resistance of material to volume change, and it can characterize the ability of material to resist deformation. In general, the larger a bulk modulus, the higher is the hardness of the compound [35]. The bulk modulus of Ni_3B, Ni_2B, Ni_4B_3, and NiB are 234.8 GPa, 256.6 GPa, 262.1 GPa, and 260.7 GPa, respectively. With the increase of B atomic ratio, bulk modulus of Ni_xB_y increases. Bulk modulus of NiB is the largest, which implies that the NiB has the highest hardness. Shear modulus and Young's modulus represent the resistance to elastic deformation (or stiffness) under shear and normal stresses. Shear modulus (122.8 GPa) and Young's modulus (318.5 GPa) of NiB are also the highest, which indicate that NiB has the greatest resistance to elastic deformation. The ratio of bulk modulus and shear modulus (B/G) can be used to judge whether a compound is brittle or ductile. The compound is ductile when the B/G value is higher than 1.75; otherwise the compound is brittle [36]. The B/G values of these Ni_xB_y compounds are all greater than 1.75, so they are all ductile. Poisson's ratio can also be used to characterize the brittleness or ductility of a material. A compound exhibits ductility (brittleness) when the Poisson's ratio is larger than (smaller than) 0.26 [37]. The Poisson's ratios are also shown in Table 3. Poisson's ratios of these Ni_xB_y compounds are all larger than 0.26, which indicates that they have good ductility. From the results of the B/G values and the Poisson's ratios, it can be found that the ductility of the Ni_xB_y compounds gradually decreases as the B atomic ratio increases.

Table 3. Bulk modulus (B), Shear modulus (G), Young's modulus (E), and Poisson's ratio (v) of the Ni_xB_y compounds.

Compounds	B_V	B_R	B	G_V	G_R	G	E	v	B/G
Ni_3B	234.8	234.7	234.8	103.2	99.8	101.5	266.2	0.311	2.313
Ni_2B	256.7	256.4	256.6	114.9	112.7	113.8	297.5	0.307	2.254
Ni_4B_3	262.1	262.1	262.1	121.0	116.5	118.8	309.2	0.308	2.276
NiB	262.9	258.4	260.7	124.7	120.9	122.8	318.5	0.296	2.122

3.2.2. Anisotropy

Anisotropy can help to understand mechanical properties of compounds [34]. Elastic anisotropy of Ni_xB_y compounds can be estimated through the elastic constants of anisotropic index. In this study, the universal anisotropic index (A^U), the percent anisotropy (A_B and A_G) are calculated to characterize the anisotropy. The equations are as follows [27]:

$$A^U = 5\frac{G_V}{G_R} + \frac{B_V}{B_R} - 6 \geq 0 \tag{10}$$

$$A_B = \frac{B_V - B_R}{B_V + B_R} \tag{11}$$

$$A_G = \frac{G_V - G_R}{G_V + G_R} \tag{12}$$

where B_V, B_R, G_V, and G_R are the bulk moduli and shear moduli obtained by the Voigt and Reuss method, respectively.

In addition, shear anisotropy needs to be considered because these Ni_xB_y compounds can assume orthorhombic and tetragonal crystal structures. The shear anisotropic factors A_1, A_2, and A_3 are defined as follows [38]:

$$A_1 = \frac{4C_{44}}{C_{11} + C_{33} - 2C_{13}} \tag{13}$$

$$A_2 = \frac{4C_{55}}{C_{22} + C_{33} - 2C_{23}} \tag{14}$$

$$A_3 = \frac{4C_{66}}{C_{11} + C_{22} - 2C_{12}} \tag{15}$$

The results of A^U, A_B, A_G, A_1, A_2, and A_3 are shown in Table 4. It can be seen from Table 4 that the values of A_1, A_2, and A_3 are not equal, which indicates that these Ni_xB_y compounds are shear anisotropic. The A_B values are very small, which indicate that these Ni_xB_y compounds have weak anisotropy in bulk modulus. A_G values of these compounds are greater than the A_B value, which suggests that the differences of shear modulus of Voigt and Reuss have a more significant impact on A^U value than bulk modulus. The larger the value of A^U, the greater is the anisotropy [39]. The A^U values of Ni_3B, Ni_2B, Ni_4B_3, and NiB are 0.167, 0.099, 0.196, and 0.174, respectively. Therefore, the order of the anisotropy for these Ni_xB_y compound is Ni_4B_3 > NiB > Ni_3B > Ni_2B. With the increase of the B atomic ratio, the anisotropy is strengthened.

Table 4. The calculated universal anisotropic index (A^U), bulk anisotropy (A_B and A_G), and shear anisotropic factors (A_1, A_2, A_3) of Ni_xB_y compounds.

Compounds	A^U	A_B	A_G	A_1	A_2	A_3
Ni_3B	0.167	0.000	0.016	1.365	1.153	1.400
Ni_2B	0.099	0.001	0.010	0.838	0.839	1.392
Ni_4B_3	0.196	0	0.019	1.230	1.231	1.425
NiB	0.174	0.009	0.015	1.433	0.777	0.994

To characterize the Young's modulus anisotropy of these Ni_xB_y compounds more intuitively, the spherical orientation is used in different directions. The directional dependence of Young's modulus for different type crystals is given by following equations [40,41]:

Orthorhombic crystal [40]

$$\begin{aligned} 1/E = {} & l_1^4 S_{11} + l_2^4 S_{22} + l_3^4 S_{33} + 2l_1^2 l_2^2 S_{12} + 2l_1^2 l_3^2 S_{13} + 2l_2^2 l_3^2 S_{23} \\ & + l_2^2 l_3^2 S_{44} + l_1^2 l_3^2 S_{55} + l_1^2 l_2^2 S_{66} \end{aligned} \tag{16}$$

Tetragonal crystal [41]

$$1/E = (l_1^4 + l_2^4) S_{11} + l_3^4 S_{33} + l_1^2 l_2^2 (2S_{12} + S_{66}) + l_3^2 (1 - l_3^2)(2S_{13} + S_{44}) + 2l_1 l_2 (l_1^2 - l_2^2) S_{16} \tag{17}$$

where S_{ij} are the elastic compliance constants, l_1, l_2 and l_3 are the directional cosines in spherical coordinates with respect to θ and φ (l_1 = sin θcos φ, l_2 = sin θsin φ, l_3 = cos φ). The more irregular the sphere, the greater is the anisotropy [42]. It can be seen from Figure 2 that the shape of Ni_4B_3 is the most irregular and Ni_4B_3 is the most regular, which indicate that the anisotropy of Ni_4B_3 is the greatest. This is consistent with above results of the anisotropy index.

The projections on the X-Y plane, X-Z plane, and Y-Z plane show more details about the anisotropy of Young's modulus as shown in Figure 3. It can be seen that the Young's modulus of these Ni_xB_y compounds have great difference in different axles. The planar contour of Ni_4B_3 is the most irregular and Ni_2B is the most regular, which indicate that the anisotropy of Ni_4B_3 is the greatest and the anisotropy of Ni_2B is the least. This is also consistent with the result of the anisotropy index presented above.

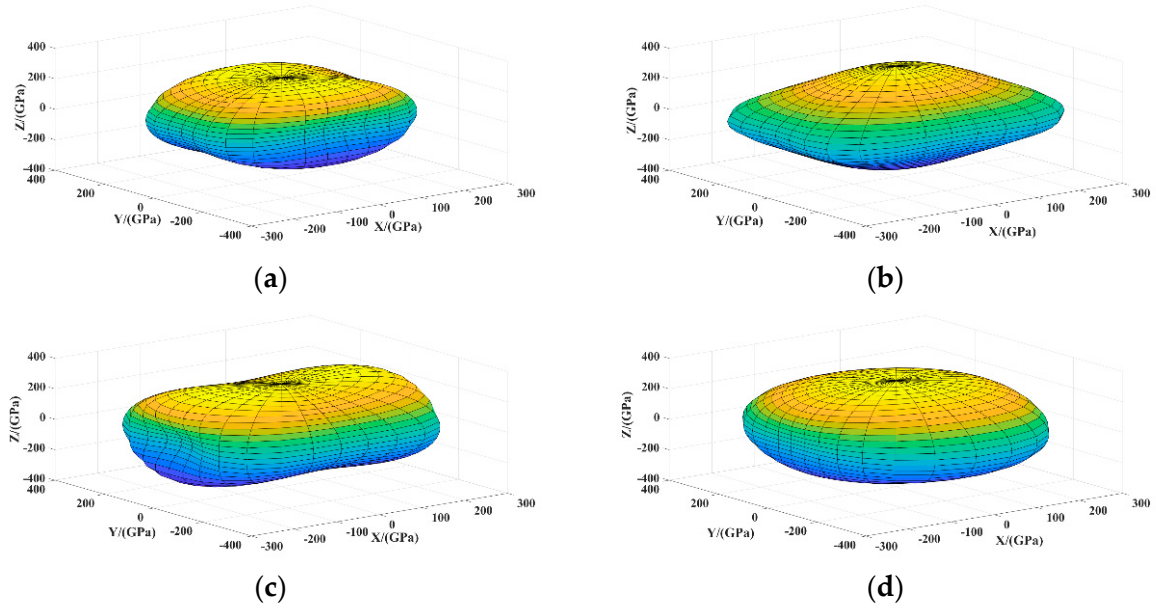

Figure 2. The surface construction of the Young's modulus of Ni_xB_y compounds (**a**) Ni_3B; (**b**) Ni_2B; (**c**) Ni_4B_3; (**d**) NiB.

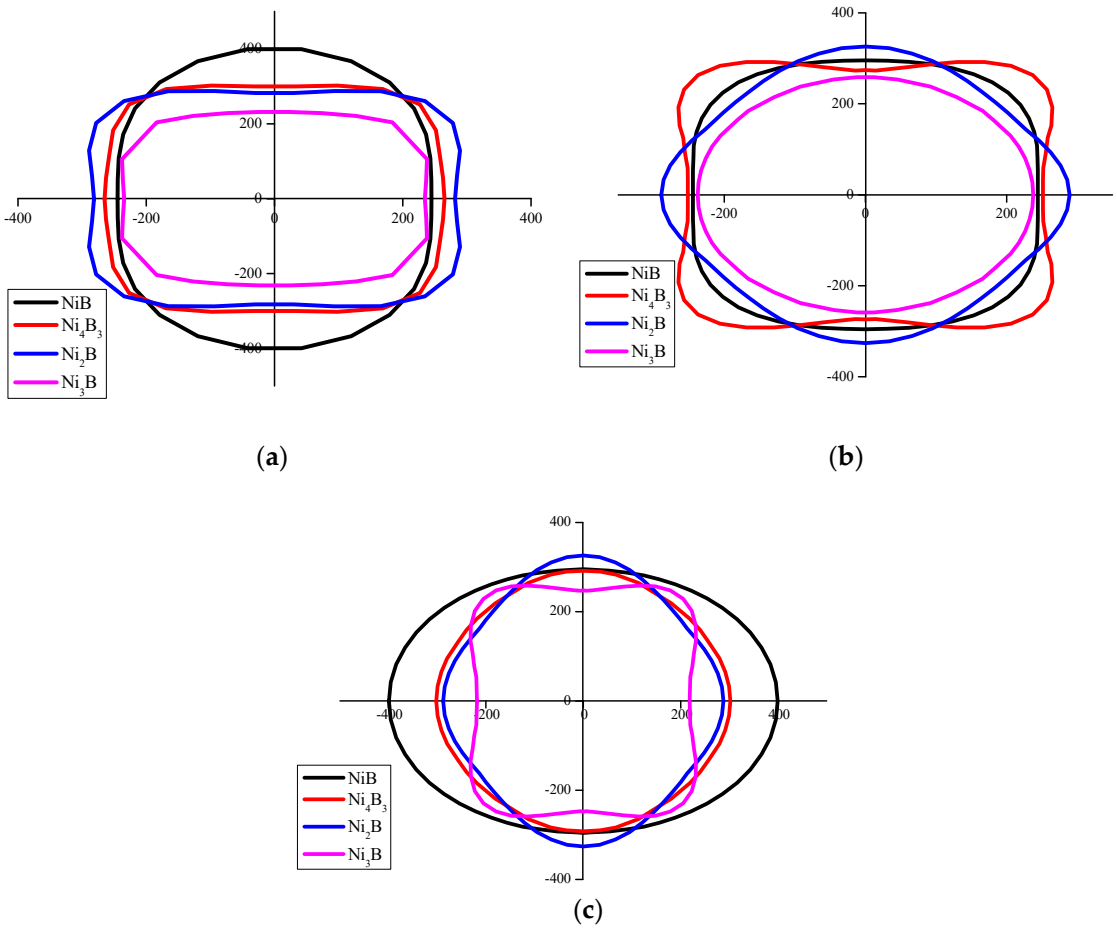

Figure 3. Planar projections of the Young's modulus of Ni_xB_y compounds (**a**) (X-Y) planar; (**b**) (X-Z) planar; (**c**) (Y-Z) planar.

3.2.3. Hardness

Hardness is an important mechanical index that reflects the resistance to localized plastic deformation of a material. In general, wear resistance of material is positively correlated with hardness, which depends on shear modulus and bulk modulus [43]. The hardness (H_V) of the Ni_xB_y compounds was calculated using the following equations [44]:

$$H_V = 2(k^2G)^{0.585} - 3 \quad (18)$$

$$\mathrm{k} = \frac{G}{B} \quad (19)$$

where G and B are shear modulus and bulk modulus, respectively.

The hardness of the Ni_xB_y compounds is shown in Figure 4. The hardness values of Ni_3B, Ni_2B, Ni_4B_3, and NiB are 8.2 GPa, 9.3 GPa, 10.0 GPa, and 10.8 GPa, respectively. NiB has the highest hardness, which is consistent with bulk modulus discussed above. With the increase of B atomic ratio, the hardness increases, which also indicates the ductility of the Ni_xB_y compound decreases.

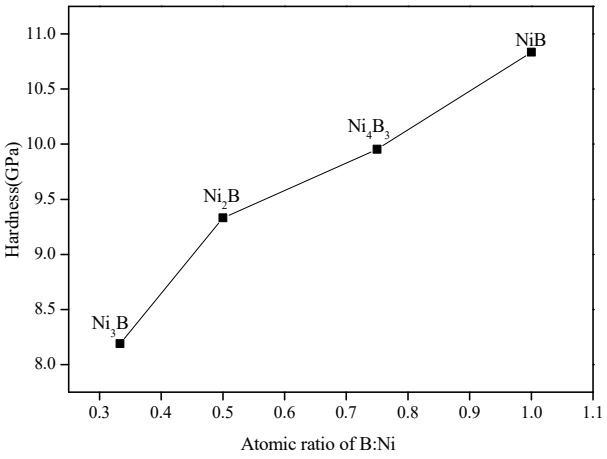

Figure 4. The hardness of Ni_xB_y compounds.

3.3. Electronic Structures

Electronic structure and characteristics of chemical bonds can be characterized by density of state (DOS). Figure 5 shows total density of states (TDOS) and partial electronic density of states (PDOS) of these Ni_xB_y compounds. Two main peaks are observed in the TDOS of Ni_xB_y compounds. The electronic structure are mainly determined by B-p band and Ni-d band. In addition, the fermi levels are also determined by Ni-d band and a small amount of B-p band, which indicates that these Ni_xB_y compounds exhibit p-d hybridization and the bond between the Ni and B atom is in the form of a covalent bond. Ni_xB_y compounds also have metal bonds because the TDOS values are greater than zero at the fermi level. Therefore, it can be concluded that the valence bonds of these Ni_xB_y compounds are composed of both metal bond and covalent bond.

The population analysis can provide more insightful information on chemical bonds of these Ni_xB_y compounds, the results are listed in Table 5. The Mulliken method is used to calculate the overlap population and the charge. Average bond strength ($\overline{L}$(AB)) and mean overlap population ($\overline{n}_{AB}$) can be calculated by the following equations [16]:

$$\overline{L}(\mathrm{AB}) = \frac{\sum_i L_i N_i}{\sum_i N_i} \quad (20)$$

$$\overline{n}_{AB} = \frac{\sum_i n_i^{AB} N_i}{\sum_i N_i} \tag{21}$$

where N_i is the total number of i bond and the L_i is the bond length of i type.

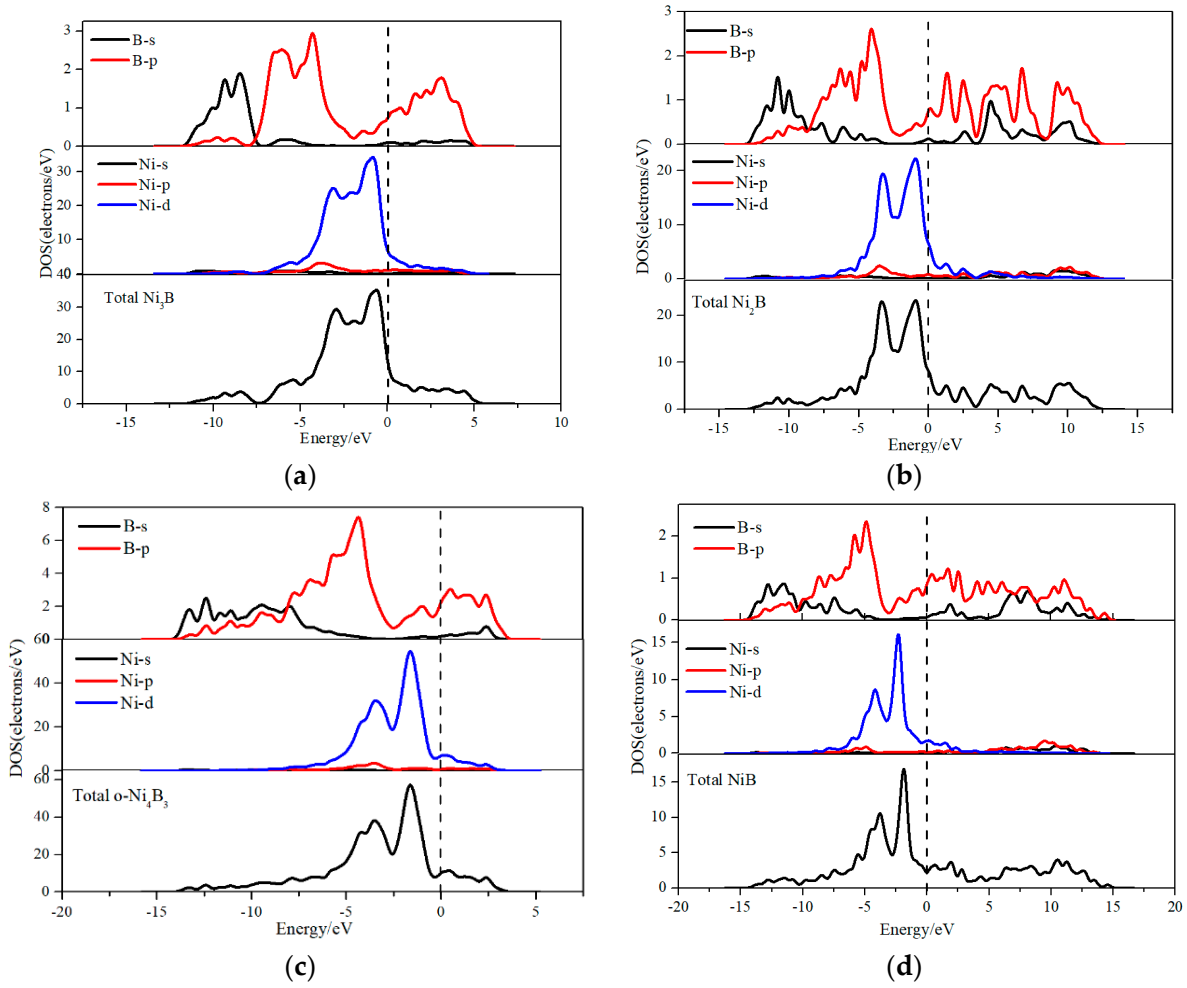

Figure 5. Total density of states (TDOS) and partial density of states (PDOS) for Ni_xB_y compounds. Dashed lines represent the Fermi level: (**a**) Ni_3B; (**b**) Ni_2B; (**c**) Ni_4B_3; (**d**) NiB.

As can be seen from Table 5, for all of the Ni_xB_y compounds, B atoms and Ni atoms carry the negative charge and the positive charge, respectively. The charge value of Ni atom varies from 0.19 (Ni_3B) to 0.54 (NiB). With the increase of B atomic ratio, the charge values of Ni in the Ni_xB_y compounds increase. There are two electron transfer paths in the Ni_xB_y compound: one is inside the Ni atom and the B atom, and the other is between the Ni atom and the B atom. The one refers to p–d hybridization covalent bond between B and Ni, and the other one is induced by the metal or weak covalent bonding among Ni atoms. In the former case, the electrons are transferred from Ni atom to B atom. The values of overlap population of Ni-Ni bond are negative, which indicate that there is an anti-bond state or strong electrostatic repulsion between Ni-Ni bond. The strengths of B-B and B-Ni covalent bonds are increased with the increase of B content. In summary, the valence bonds of these Ni_xB_y compounds are composed of the metal bond and the covalent bond.

Table 5. Milliken population analysis results of Ni_xB_y, the unit of bond length is Å.

Species	Atoms	s	p	d	Total Electrons	Charge
Ni_3B	B	1.12	2.46		3.58	−0.58
	Ni	0.35	0.73	8.72	9.81	0.19
Ni_2B	B	1.07	2.45		3.52	−0.52
	Ni	0.30	0.72	8.72	9.74	0.26
Ni_4B_3	B	1.00	2.50		3.53	−0.53
	Ni	0.24	0.63	8.73	9.60	0.40
NiB	B	0.99	2.55		3.54	−0.54
	Ni	0.18	0.55	8.73	9.46	0.54
Species	**Bond**	**$\bar{L}$(AB) (Å)**			**$\overline{n_{AB}}$(*electrons*)**	
Ni_3B	B-Ni	2.11			0.28	
	Ni-Ni	2.56			−0.01	
Ni_2B	B-B	2.14			0.65	
	B-Ni	2.14			0.15	
	Ni-Ni	2.59			−0.11	
Ni_4B_3	B-B	2.33			0.76	
	B-Ni	2.30			0.17	
	Ni-Ni	2.93			−0.13	
NiB	B-B	1.78			1.45	
	B-Ni	2.15			0.28	
	Ni-Ni	2.61			−0.14	

3.4. Debye Temperature

During the laser cladding process, compound undergoes rapid heating and cooling, so studying the thermodynamic properties of the material is very important. Debye temperature and sound velocity are important parameters for thermodynamic properties, which are related to the chemical bonding characteristics and thermal properties of Ni_xB_y compounds [45]. Debye temperature and sound velocity can be calculated by following equations [46–48]:

$$\Theta_D = \frac{h}{k_B}\left[\frac{3n}{4\pi}\left(\frac{N_A\rho}{M}\right)\right]^{1/3} v_m \tag{22}$$

$$v_m = \left[\frac{1}{3}\left(\frac{2}{{v_s}^3} + \frac{1}{{v_1}^3}\right)\right]^{-1/3} \tag{23}$$

$$v_1 = \left[\left(B + \frac{4}{3}G\right)\frac{1}{\rho}\right]^{1/2} \tag{24}$$

$$v_s = (G/\rho)^{1/2} \tag{25}$$

where h, k_B, n, ρ, N_A, and M are, respectively, the Planck constant, Boltzmann constant, the number of atoms, the density, the Avogadro constant, and the molar mass of the compound. v_m, v_1, and v_s are respectively the average speed of sound, the velocity of the longitudinal sound and transverse velocity.

The values of Debye temperatures and sound velocities of Ni_3B, Ni_2B, Ni_4B_3, and NiB are calculated and listed in Table 6. The order of Debye temperatures for Ni_xB_y compounds are NiB > Ni_4B_3 > Ni_2B > Ni_3B. The Debye temperature of NiB is the highest (681.8 K), so the thermodynamic stability of NiB is superior to other Ni-B compounds. With the increase of the B atomic ratio, the Debye temperatures of these Ni_xB_y compounds increase. The longitudinal velocity and transverse velocity are correlated to the bulk modulus, shear modulus, and the density of the compound. The compounds with large bulk modulus and the low density will have large sound velocity. Hence, NiB has the highest sound velocity among these Ni_xB_y compounds because it has the highest shear modulus and bulk modulus. This conclusion can also be used to explain the sound velocity of other compounds.

Table 6. Theoretically calculated thermal properties of the Ni_xB_y compounds, including v_s, v_1, v_m, and Θ_D.

Compounds	v_s/m·s^{-1}	v_1/m·s^{-1}	v_m/m·s^{-1}	Θ_D/K
Ni_3B	3505.6	6693.7	3921.2	553.4
Ni_2B	3663.8	6939.4	4095.9	600.7
Ni_4B_3	3958.1	7447.8	4422.9	645.1
NiB	4052.4	7532.9	4524.4	681.8

4. Conclusions

In this study, the results showed that mechanical properties, electronic properties, and Debye temperature of Ni_xB_y compounds with different atomic ratios are different. This can provide theoretical guidance for material design in the laser cladding layer and help to account for changes in performance under different Ni and B ratios. The conclusions are drawn as follows:

(1) The calculated lattice parameters are consistent with the predecessor calculation data. The formation energy of all Ni_xB_y compounds is negative, which indicates that all Ni_xB_y compounds have stable structures.

(2) Ni_xB_y compounds have mechanical stability. NiB has the largest bulk modulus, shear modulus and Young's modulus and the smallest Poisson's ratio, which imply that the hardness of NiB is higher than other Ni_xB_y compounds. Ni_xB_y compounds exhibit anisotropic characteristics, and Ni_4B_3 had the greatest anisotropy. The mechanical properties of the Ni_xB_y compounds increase with the increase of the B atomic ratio.

(3) Ni_xB_y compounds exhibit p-d hybridization and they exhibit the metal bond and the covalent bond.

(4) NiB has largest Debye temperature (7681.8 K), which indicates that NiB has the highest thermodynamic stability. Debye temperature of the Ni_xB_y compounds increase with the increase of the B atomic ratio.

Author Contributions: K.W., D.D. and B.C. conceived and designed the experiments; K.W. and Y.H. performed the experiments; K.W., J.J. and S.S. analyzed the data; H.F. contributed reagents/materials/analysis tools; K.W. and B.C. wrote the paper.

Funding: This research was funded by [National Natural Science Foundation of China] grant number [51675303], [National Natural Science Foundation of China] grant number [51605251], [National Key Research and Development Program of China] grant number [2017YFB1103303], and [the Tribology Science Fund of the State Key Laboratory of Tribology] grant number [SKLT2018B05].

Acknowledgments: The authors appreciate the financial support to this work from National Natural Science Foundation of China (No.51675303, No51605251), National Key Research and Development Program of China (2017YFB1103303), and the Tribology Science Fund of the State Key Laboratory of Tribology (SKLT2018B05).

Conflicts of Interest: The authors declare no conflict of interest.

References

1. Farahmand, P.; Liu, S.; Zhang, Z.; Kovacevic, R. Laser cladding assisted by induction heating of Ni–WC composite enhanced by nano-WC and La_2O_3. *Ceram. Int.* **2014**, *40*, 15421–15438. [CrossRef]
2. Wang, K.; Fu, H.; Li, Y.; Lei, Y.; Wei, S.; Su, Z. Effect of power on microstructure and properties of laser cladding NiCrBSi composite coating. *Trans. Inst. Met. Finish.* **2017**, *95*, 328–336.
3. Chen, C.H.; Bai, Y.; Chen, W.; Ye, X.C. Boron Influence on Structures and Properties in Nickel-Based Alloys. *Appl. Mech. Mater.* **2013**, *395–396*, 251–258. [CrossRef]
4. González, R.; García, M.A.; Peñuelas, I.; Cadenas, M.; Fernández, M.D.R.; Battez, A.H.; Felgueroso, D. Microstructural study of NiCrBSi coatings obtained by different processes. *Wear* **2007**, *263*, 619–624. [CrossRef]
5. Ma, Q.; Li, Y.; Wang, J.; Liu, K. Investigation on cored-eutectic structure in Ni60/WC composite coatings fabricated by wide-band laser cladding. *J. Alloys Compd.* **2015**, *645*, 151–157. [CrossRef]

6. Wu, Z.J.; Ge, S.H.; Zhang, M.H.; Li, W.; Mu, S.C.; Tao, K.Y. Controlled Synthesis of Supported Nickel Boride Catalyst Using Electroless Plating. *J. Phys. Chem. C* **2007**, *111*, 8587–8593. [CrossRef]
7. Choi, J.W.; Hwang, G.H.; Han, W.K.; Kang, S.G. Phase transformation of Ni-B, Ni-P diffusion barrier deposited electrolessly on Cu interconnect. *Appl. Surf. Sci.* **2006**, *253*, 2171–2178. [CrossRef]
8. Eraslan, S.; Ürgen, M. Oxidation behavior of electroless Ni-P, Ni-B and Ni-W-B coatings deposited on steel substrates. *Surf. Coat. Technol.* **2015**, *265*, 46–52. [CrossRef]
9. Anik, M.; Körpe, E.; Şen, E. Effect of coating bath composition on the properties of electroless nickel–boron films. *Surf. Coat. Technol.* **2008**, *202*, 1718–1727. [CrossRef]
10. Wang, K.; Chang, B.; Chen, J.; Fu, H.; Lin, Y.; Lei, Y. Effect of Molybdenum on the Microstructures and Properties of Stainless Steel Coatings by Laser Cladding. *Appl. Sci.* **2017**, *7*, 1065. [CrossRef]
11. Hou, X.; Du, D.; Wang, K.; Hong, Y.; Chang, B. Microstructure and Wear Resistance of Fe-Cr-Mo-Co-CB Amorphous Composite Coatings Synthesized by Laser Cladding. *Metals* **2018**, *8*, 622. [CrossRef]
12. Li, Q.; Lei, Y.; Fu, H. Growth mechanism, distribution characteristics and reinforcing behavior of (Ti, Nb)C particle in laser cladded Fe-based composite coating. *Appl. Surf. Sci.* **2014**, *316*, 610–616. [CrossRef]
13. Wang, K.; Chang, B.; Lei, Y.; Fu, H.; Lin, Y. Effect of Cobalt on Microstructure and Wear Resistance of Ni-Based Alloy Coating Fabricated by Laser Cladding. *Metals* **2017**, *7*, 551. [CrossRef]
14. Liu, Y.; Xing, J.; Li, Y.; Sun, L.; Wang, Y. A first principles study of adhesion and electronic structure at Fe (110)/graphite (0001) interface. *Appl. Surf. Sci.* **2017**, *405*, 497–502. [CrossRef]
15. Shein, I.R.; Medvedeva, N.I.; Ivanovskii, A.L. Electronic and structural properties of cementite-type M_3X (M = Fe, Co, Ni; X = C or B) by first principles calculations. *Physica B* **2006**, *371*, 126–132. [CrossRef]
16. Zhou, C.T.; Xing, J.D.; Xiao, B.; Feng, J.; Xie, X.J.; Chen, Y.H. First principles study on the structural properties and electronic structure of X_2B (X = Cr, Mn, Fe, Co, Ni, Mo and W) compounds. *Comp. Mater. Sci.* **2009**, *44*, 1056–1064. [CrossRef]
17. Zhou, Y.; Xiang, H.; Feng, Z.; Li, Z. Electronic Structure and Mechanical Properties of NiB: A Promising Interphase Material for Future UHTCf/UHTC Composites. *J. Am. Ceram. Soc.* **2016**, *99*, 2110–2119. [CrossRef]
18. Wang, K.; Li, Y.; Fu, H.; Lei, Y.; Su, Z.; Ma, P. A study of laser cladding NiCrBSi/Mo composite coatings. *Surf. Eng.* **2018**, *34*, 267–275.
19. Liu, K.; Fan, H.; Ren, P.; Yang, C. Structural, electronic and optical properties of $BiFeO_3$ studied by first-principles. *J. Alloys Compd.* **2011**, *509*, 1901–1905. [CrossRef]
20. Skylaris, C.K. A benchmark for materials simulation. *Science* **2016**, *351*, 1394–1395. [CrossRef] [PubMed]
21. Ravi, C. First-principles study of crystal structure and stability of AlMgSi(Cu) precipitates. *Acta Mater.* **2004**, *52*, 4213–4227. [CrossRef]
22. Connétable, D.; Thomas, O. First-principles study of the structural, electronic, vibrational, and elastic properties of orthorhombic NiSi. *Phys. Rev. B* **2009**, *79*, 094101. [CrossRef]
23. Schaefer, Z.L.; Ke, X.; Schiffer, P.; Schaak, R.E. Direct Solution Synthesis, Reaction Pathway Studies, and Structural Characterization of Crystalline Ni3B Nanoparticles. *J. Phys. Chem. C* **2008**, *112*, 19846–19851. [CrossRef]
24. Kong, Y.; Xiong, W.; Guo, H.; Sun, W.; Du, Y.; Zhou, Y. Elastic and thermodynamic properties of the Ni–B system studied by first-principles calculations and experimental measurements. *Calphad* **2010**, *34*, 245–251. [CrossRef]
25. Fujimori, M.; Nakata, T.; Nakayama, T.; Nishibori, E.; Kimura, K.; Takata, M.; Sakata, M. Peculiar covalent bonds in alpha-rhombohedral boron. *Phys. Rev. Lett.* **1999**, *82*, 4452–4455. [CrossRef]
26. Liu, Y.H.; Chong, X.Y.; Jiang, Y.H.; Zhou, R.; Feng, J. Mechanical properties and electronic structures of Fe-Al intermetallic. *Physica B* **2017**, *506*, 1–11. [CrossRef]
27. Xiao, B.; Feng, J.; Zhou, C.T.; Jiang, Y.H.; Zhou, R. Mechanical properties and chemical bonding characteristics of Cr_7C_3 type multicomponent carbides. *J. Appl. Phys.* **2011**, *109*, 023507. [CrossRef]
28. Li, Y.; Gao, Y.; Xiao, B.; Min, T.; Fan, Z.; Ma, S.; Xu, L. Theoretical study on the stability, elasticity, hardness and electronic structures of W–C binary compounds. *J. Alloys Compd.* **2010**, *502*, 28–37. [CrossRef]
29. Maibam, J.; Indrajit Sharma, B.; Bhattacharjee, R.; Thapa, R.K.; Brojen Singh, R.K. Electronic structure and elastic properties of scandium carbide and yttrium carbide: A first principles study. *Physcia B* **2011**, *406*, 4041–4045. [CrossRef]
30. Feng, J.; Xiao, B.; Chen, J.; Du, Y.; Yu, J.; Zhou, R. Stability, thermal and mechanical properties of PtxAly compounds. *Mater. Des.* **2011**, *32*, 3231–3239. [CrossRef]

31. Qi, C.J.; Jiang, Y.H.; Liu, Y.Z.; Zhou, R. Elastic and electronic properties of XB_2 (X = V, Nb, Ta, Cr, Mo, and W) with AlB_2 structure from first principles calculations. *Ceram. Int.* **2014**, *40*, 5843–5851. [CrossRef]
32. Feng, J.; Xiao, B.; Zhou, R.; Pan, W.; Clarke, D.R. Anisotropic elastic and thermal properties of the double perovskite slab–rock salt layer $Ln_2SrAl_2O_7$ (Ln = La, Nd, Sm, Eu, Gd or Dy) natural superlattice structure. *Acta Mater.* **2012**, *60*, 3380–3392. [CrossRef]
33. Pathak, A.; Mehta, K.K.; Singh, A.K. A first principles calculation of Ni-16Cr and Ni-16Mo alloys. *J. Appl. Res. Technol.* **2017**, *15*, 78–82. [CrossRef]
34. Sun, S.; Fu, H.; Lin, J.; Guo, G.; Lei, Y.; Wang, R. The stability, mechanical properties, electronic structures and thermodynamic properties of (Ti, Nb)C compounds by first-principles calculations. *J. Mater. Res.* **2018**, *33*, 495–506. [CrossRef]
35. Ozisik, H.; Deligoz, E.; Colakoglu, K.; Surucu, G. Structural and mechanical stability of rare-earth diborides. *Chin. Phys. B* **2013**, *22*, 369–376. [CrossRef]
36. Liu, Y.; Xing, J.; Fu, H.; Li, Y.; Sun, L.; Lv, Z. Structural stability, mechanical properties, electronic structures and thermal properties of XS (X = Ti, V, Cr, Mn, Fe, Co, Ni) binary compounds. *Phys. Lett. A* **2017**, *381*, 2648–2657. [CrossRef]
37. Özışık, H.; Çiftci, Y.Ö.; Çolakoğlu, K.; Deligöz, E. The structural, elastic and vibrational properties of the DyX (X = P, As) compounds. *Phys. Scr.* **2011**, *83*, 035601. [CrossRef]
38. Lee, E.; Lee, B.J. Modified embedded-atom method interatomic potential for the Fe-Al system. *J. Phys. Condens. Matter.* **2010**, *22*, 175702. [CrossRef] [PubMed]
39. Yan, P.; Chong, X.; Jiang, Y.; Feng, J. Effects of alloying elements such as Ti, Zr and Hf on the mechanical and thermodynamic properties of Pd-Base superalloy. *J. Alloys Compd.* **2017**, *710*, 589–599. [CrossRef]
40. Feng, J.; Xiao, B.; Zhou, R.; Pan, W. Anisotropy in elasticity and thermal conductivity of monazite-type $REPO_4$ (RE = La, Ce, Nd, Sm, Eu and Gd) from first-principles calculations. *Acta Mater.* **2013**, *61*, 7364–7383. [CrossRef]
41. Nye, J.F. *Physical Properties of Crystals: Their Representation by Tensors and Matrices*; Oxford University Press: Oxford, UK, 1985.
42. Liu, Y.; Jiang, Y.; Feng, J.; Zhou, R. Elasticity, electronic properties and hardness of MoC investigated by first principles calculations. *Physcia B* **2013**, *419*, 45–50. [CrossRef]
43. Sun, S.; Liu, Y.; Fu, H.; Guo, X.; Ma, S.; Lin, J.; Guo, G.; Lei, Y.; Wang, R. First Principles Study of Mechanical Properties and Electronic Structures of Vanadium-Doped TiC and TiN. *Adv. Eng. Mater.* **2018**, *20*, 1800295. [CrossRef]
44. Chen, X.; Niu, H.; Li, D.; Li, Y. Modeling hardness of polycrystalline materials and bulk metallic glasses. *Intermetallics* **2011**, *19*, 1275–1281. [CrossRef]
45. Deligoz, E.; Ciftci, Y.O.; Jochym, P.T.; Colakoglu, K. The first principles study on PtC compound. *Mater. Chem. Phys.* **2008**, *111*, 29–33. [CrossRef]
46. Chen, C.L.; Lu, W.; He, L.L.; Ye, H.Q. First-principles study of deformation-induced phase transformations in Ti-Al intermetallics. *J. Mater. Res.* **2009**, *24*, 1662–1666. [CrossRef]
47. Feng, J.; Xiao, B.; Wan, C.L.; Qu, Z.X.; Huang, Z.C.; Chen, J.C.; Zhou, R.; Pan, W. Electronic structure, mechanical properties and thermal conductivity of $Ln_2Zr_2O_7$ (Ln = La, Pr, Nd, Sm, Eu and Gd) pyrochlore. *Acta Mater.* **2011**, *59*, 1742–1760. [CrossRef]
48. Liu, L.; Xu, G.; Wang, A.; Wu, X.; Wang, R. First-principles investigations on structure stability, elastic properties, anisotropy and Debye temperature of tetragonal LiFeAs and NaFeAs under pressure. *J. Phys. Chem. Solids* **2017**, *104*, 243–251. [CrossRef]